Journal of Ceramic Processing Research. Vol. 20, No. 1, pp. 59~62 (2019)

J O U R N A L O F
Ceramic Processing Research

Influence of the SPS heating rate on the optical and mechanical properties of Y_2O_3-MgO nanocomposites

Seok-Min Yong*, Doo Hyun Choi, Kisu Lee, Seok-Young Ko and Dong-Ik Cheong
Agency for Defense Development (ADD), Yuseong P.O. Box 35, Daejeon 34816, Korea

Y_2O_3-MgO nanocomposites are promising materials for hypersonic infrared windows and domes due to their excellent mid-IR transmittance and mechanical properties. In this work, influence of SPS heating rate on the microstructure, IR transmittance, and mechanical properties of Y_2O_3-MgO nanocomposites was investigated. It was found that the average grain size decreases with a decreasing heating rate, which can be attributed to high defect concentration by rapid heating and deformation during densification. Also, the residual porosity decreases with a decreasing heating rate, which is ascribed to the enhancement of grain boundary diffusion by a large grain-boundary area (a small grain size). Consequently, high transmittance and hardness were attained by the low heating rate. On the other hand, the mechanical strength showed little difference with the heating rate change, which is somewhat different from the general knowledge on ceramics and will be discussed in this letter.

Key words: Infrared transparent ceramics, Y_2O_3-MgO nanocomposite, Spark plasma sintering, Heating rate.

Introduction

Y_2O_3-MgO nanocomposites have recently received considerable attention as one of the most promising candidate materials for hypersonic infrared (IR) windows and domes due to their excellent MWIR transmittance and mechanical properties [1-4]. In these nanocomposites, the presence of one phase naturally impedes the grain growth of the adjacent phase. This is known as the pinning effect, and this is most effective when the phases have comparable volume fractions and are dispersed uniformly in the composites. The reduced grain size can increase the optical transparency, especially when the grain size is smaller than the wavelength of the incident light (less than approximately $\lambda/20$). In addition, a smaller grain size increases the mechanical strength and thermal shock resistance [5, 6]. Thus, Y_2O_3-MgO nanocomposites exhibit optical and mechanical properties superior to those of other IR transparent materials, such as Al_2O_3, $MgAl_2O_4$, AlON, and Y_2O_3 [7].

It is difficult, however, to obtain excellent optical and mechanical properties with Y_2O_3-MgO nanocomposites when using the conventional pressureless sintering process. Kear et al. [5] reported that a sample sintered in air at 1600 ºC for 5 h showed a density level of less than 95%. After re-heating to 1700 ºC in air for 5 h, the density increased to nearly 100%, but the grain size increased to approximately 10 μm. In general, therefore, the densification of transparent nanocomposites is conducted using special sintering techniques, such as hot pressing (HP), hot isostatic pressing (HIP), and spark plasma sintering (SPS). The SPS technique has significant advantages over HP and HIP because it can complete the densification within a short sintering time owing to the application of a high electric field (typical heating rate > 50 ºC/min) [8-10]. A few studies of the SPS of Y_2O_3-MgO nanocomposite have been reported. Xu et al. [11] and Jiang et al. [12] studied the influence of SPS and the post-sinter annealing conditions on the optical transmittance of these composites. Huang et al. [13] investigated the effect of SPS temperature on the mechanical properties.

Recently, many researchers have reported that, for the SPS processing of polycrystalline transparent materials, a low heating rate is efficient for densification and transparency. Kim et al. [14] reported that the α-Al_2O_3 sintered at 1150 ºC with a heating rate of 8 ºC/min has a residual porosity of 0.03% and in-line transmission of 47% at a wavelength of 640 nm. Morita et al. [8] reported that a light transmission of 47% at a wavelength of 550 nm and a fracture strength of ~500 MPa for $MgAl_2O_4$ spinel sintered at 1300 ºC with a heating rate of < 10 ºC/min. In this study, the influence of the SPS heating rate on the microstructure, IR transmittance, and mechanical properties of the Y_2O_3-MgO nanocomposites was investigated.

Experimental

Y_2O_3-MgO nanopowder was synthesized using the sol-gel combustion method. Details of the nanopowder

*Corresponding author:
Tel : +82-42-821-0924
Fax: +82-42-821-3400
E-mail: y990906@hanmail.net

synthesis approach are described in the literature [1]. Yttrium nitrate ($Y(NO_3)_3 \cdot 6H_2O$) and magnesium acetate ($(CH_3COO)_2Mg \cdot 4H_2O$), corresponding to Y_2O_3 and MgO at a volume ratio of 50:50, were dissolved in deionized water under mild magnetic stirring at room temperature. The above solution was dried in a preheated electric oven at 200 °C for 36 h. The dried gel was then heated in a box furnace to 1000 °C (heating rate of 5 °C/min) with a holding time of 2 h. The heat-treated powder was ball-milled with ZrO_2 balls in anhydrous alcohol for 24 h. The slurry was dried at 80 °C and sieved through a 200-mesh screen.

Densification of the as-prepared composite nanopowder was carried out using a SPS system under a vacuum (~6 Pa). The composite nanopowder was loaded into a graphite die with graphite foils at both ends, and heated from room temperature to 1300 °C at a heating rate of 5 ~ 100 °C/min under uniaxial pressure of 50 MPa. It was held for 5 min before turning off the power. The temperature was controlled by an optical pyrometer focused on the outer surface of the graphite die. Post-sinter annealing was conducted at 1100 °C for 20 h in air. The annealed samples were then mirror-polished on both surfaces for further characterization and investigation.

The crystallite phase of the synthesized nanopowder and the sintered samples was characterized by X-ray diffractometer (XRD, D/MAX-2500, Rigaku, Japan) with Cu Kα radiation. The microstructure of the sintered samples was examined by scanning electron microscopy (FE-SEM, Quanta 650, FEI, Netherlands). For the SEM observation, mirror-polished samples were thermally etched at 1100 °C for 1 h in air. The grain size was determined by counting the number of grains in the SEM micrograph. Assuming the grains to be spherical, the average grain size was determined to be 1.225 times the apparent grain size [15]. Fourier transform infrared spectroscopy (FTIR, Nicolet iS50, Thermo Scientific, USA) was used to measure the transmittance of the sintered sample in a wavelength range of 2.5 ~ 10 μm. The hardness was measured using a Vickers hardness tester (VLPAK2000. Mitutoyo, Japan) with a load of 1 kg on the surface. Mechanical strength was measured in accordance with ASTM C-1499 using and Instron 5882 machine (Instron, USA). Support and road ring diameters were 10.5 and 5.5 mm. The diameter and the thickness of the test specimens were 20 and 1 mm, respectively.

In this paper, YM-X denotes the Y_2O_3-MgO nanocomposite sintered with a heating rate of X °C/min.

Results and Discussion

The XRD patterns of the synthesized Y_2O_3-MgO nanopowder and fabricated Y_2O_3-MgO nanocomposites are displayed in Fig. 1. It is clearly observed that all the samples are composed of cubic Y_2O_3 (JCPDS No. 72-

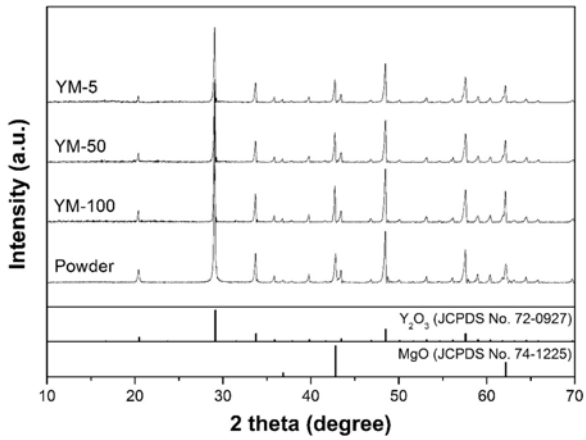

Fig. 1. The XRD patterns of the synthesized Y_2O_3-MgO nanopowder and fabricated Y_2O_3-MgO nanocomposites.

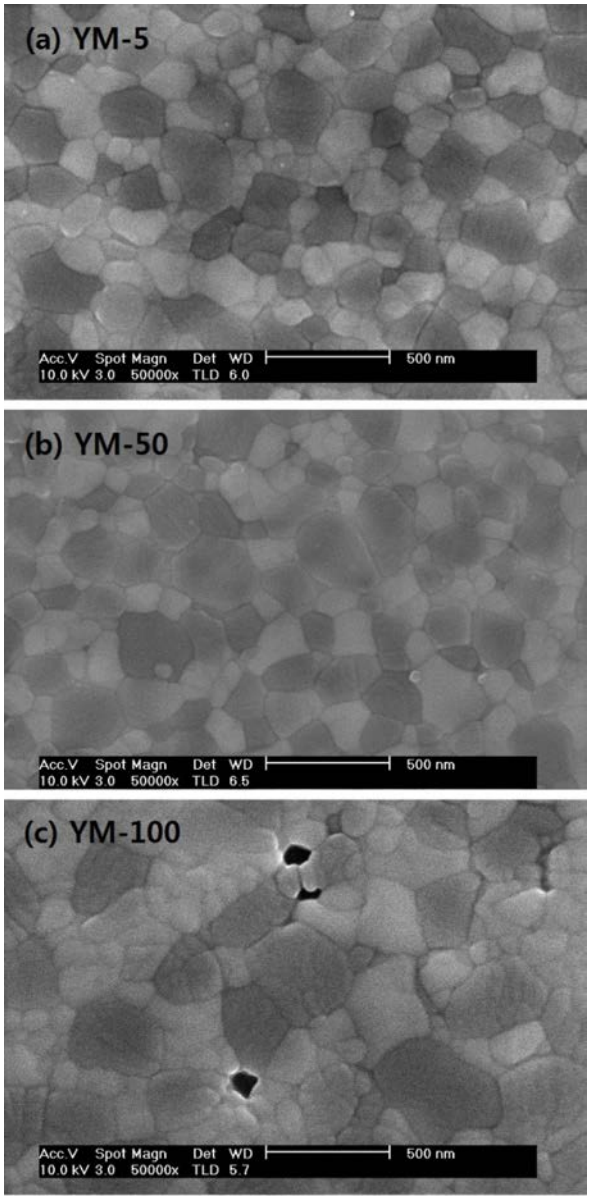

Fig. 2. SEM micrographs of the fabricated Y_2O_3-MgO nanocomposites: (a) YM-5, (b) YM-50, and (c) YM-100.

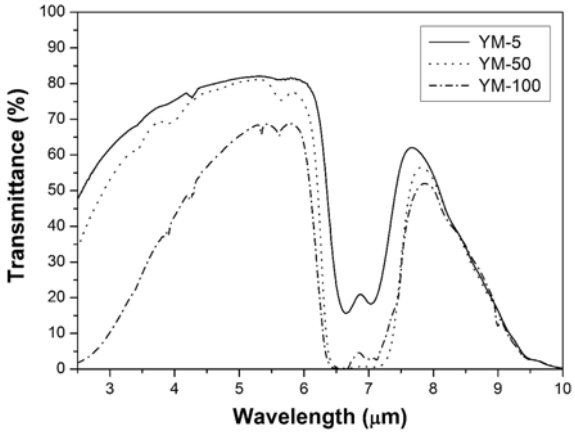

Fig. 3. IR transmittance spectra of the fabricated Y_2O_3-MgO nanocomposites.

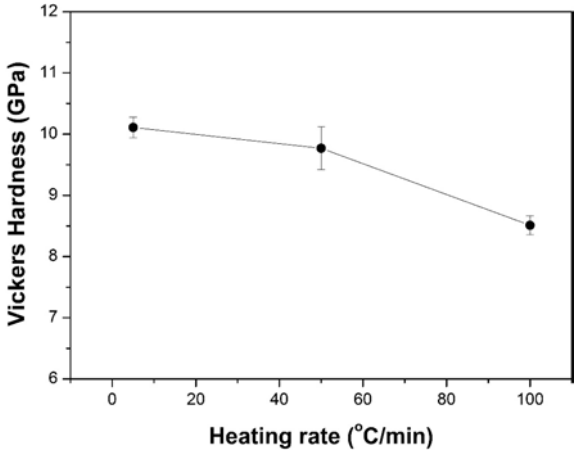

Fig. 4. Vickers hardness values of the fabricated Y_2O_3-MgO nanocomposites.

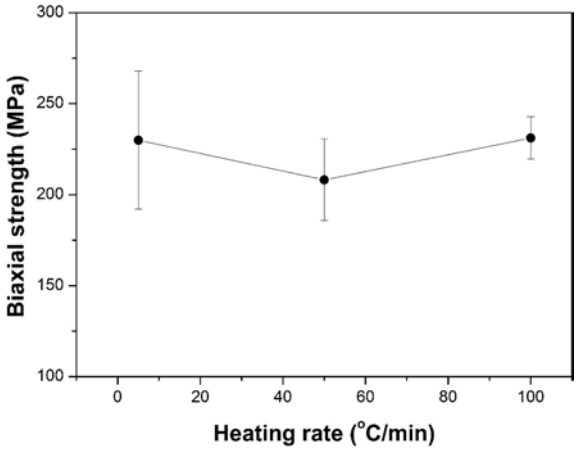

Fig. 5. Biaxial strength values of the fabricated Y_2O_3-MgO nanocomposites.

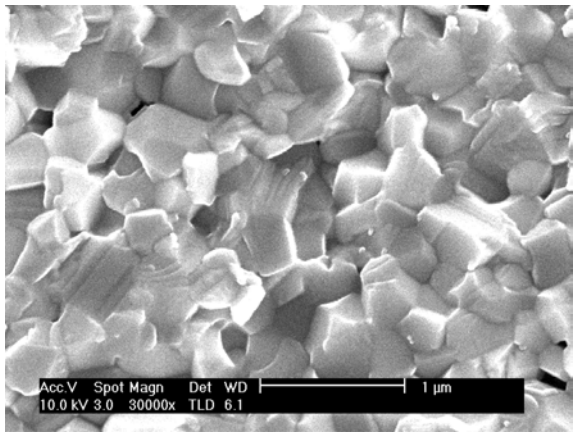

Fig. 6. SEM micrograph showing the fracture surfaces of YM-100.

0927) and MgO (JCPDS No. 74-1225) phases. Other materials as impurities were not found.

The SEM micrographs of the fabricated Y_2O_3-MgO nanocomposites are shown in Fig. 2. The bright grains are the Y_2O_3 phase and the dark grains are the MgO phase. It is confirmed that the heating rate strongly affects the grain size and residual porosity. The average grain size decreases with a decreasing heating rate (168.1, 173.2, and 247.6 nm for YM-5, 50, and 100, respectively), which can be attributed to high defect concentration produced by rapid heating and associated rapid deformation during densification. Large DC current for rapid heating is considered to assist the defect formation owing to high-temperature plasma generated on particle surfaces, and the deformation-induced defects are known to induce dynamic grain growth. The defects produced by both heating and deformation may therefore accelerate the grain growth during SPS processing [16]. The residual porosity also decreases with a decreasing heating rate, which agrees well with the measured relative densities (99.7, 99.1, and 97.1% for YM-5, 50, and 100, respectively). For YM-5, it is difficult to observe residual pores, which indicates that densification is almost completed. For YM-50, although few residual pores of < 50 nm are occasionally observed at the grain boundary junctions, the fraction of pores is significantly lower. For YM-100, numerous residual pores of ~ 100 nm or larger are frequently observed at the grain boundary junctions. The effect of the heating rate can be explained by grain-boundary diffusion. Since a small grain size means a large grain-boundary area, the large boundary area along with the low porosity for slow heating may enhance grain boundary diffusion and eventually densification. In addition, the small grain size lowers the flow stress for grain boundary sliding, and hence, deformation-induced densification can also be activated [16, 17].

Fig. 3 shows the IR transmittance spectra of the fabricated Y_2O_3-MgO nanocomposites. YM-5 exhibits the highest transmittance in the mid-IR range. The transmittance decreases with increasing heating rate (81.5, 80.4, and 65.4% at 5 μm for YM-5, 50, and 100, respectively). This may be attributed to the increase of not only the grain boundary scattering stemming from

the relatively large grain size but also the scattering at the pores caused by the large difference in the refractive index between the nanocomposite and the pores [5, 7]. The absorption peak near 7 μm is attributed to asymmetrical and symmetrical stretching vibrations of the carboxylate group, which is contributed to not only residual carbonate after calcination and annealing but also carbon contamination from the graphite die. A weak absorption peak at 4.28 μm is associated with CO_2 in the environment [18].

The measured Vickers hardness and biaxial strength values of the fabricated Y_2O_3-MgO nanocomposites are shown in Fig. 4 and 5, respectively. The average hardness decreases with increasing the heating rate (10.1, 9.8, and 8.5 GPa for YM-5, 50, and 100, respectively). In general, the mechanical properties of the polycrystalline ceramic are mainly influenced by the grain size and porosity. For a large grain size, a small number of grain boundaries cannot act as obstacles to dislocation movement, resulting in low hardness levels (Hall-Petch relationship [13]). Moreover, high porosity leads to a decrease in the hardness. For the biaxial strength, on the other hand, there is no pronounced relationship with the grain size and porosity resulting from the different heating rate (229.9, 208.1, and 231.2 MPa for YM-5, 50, and 100, respectively). These results indicate that there is another factor affecting the mechanical strength. Fig. 6 displays a SEM micrograph showing the fracture surfaces of YM-100. The fracture of YM-100 is dominated by intergranular fracture. The other samples (YM-5 and 10) also exhibit the same fracture trend as YM-100. The fracture of all samples is dominated by intergranular fracture. It is presumed that this intergranular fracture can be ascribed to the presence of a residual amorphous carbon phase along the grain boundaries caused by the carbon contamination during the SPS processing [19]. As a similar case, it has been previously reported that the hot-pressed Y_2O_3-MgO nanocomposite fabricated using the graphite die also exhibits the constant mechanical strength value regardless of the grain size and residual pores [19], which supports the above presumption. Therefore, further analysis of the grain boundary phase might be required to improve the mechanical strength of Y_2O_3-MgO nanocomposite fabricated by the SPS process.

Conclusions

In this work, the influence of SPS heating rate on the microstructure, IR transmittance, and mechanical properties of Y_2O_3-MgO nanocomposites was investigated. The average grain size and residual porosity decreased with decreasing heating rate, leading to improvement of the mechanical hardness and the transmittance in the mid-IR range. However, the mechanical strength was not influenced by the grain size and porosity resulting from different heating rate, and further studies are required to identify the reason. These results indicate that the SPS heating rate is a very important factor determining the optical performance of the Y_2O_3-MgO nanocomposite.

Acknowledgements

This work was supported by DAPA and ADD.

References

1. J. Wang, D. Chen, E.H. Jordan, and M. Gell, J. Am. Ceram. Soc. 93[11] (2010) 3535-3538.
2. S. Xu, J. Li, C. Li, Y. Pan, and J. Guo, J. Am. Ceram. Soc. 98[3] (2015) 1019-1026.
3. S. Xu, J. Li, C. Li, Y. Pan, and J. Guo, J. Am. Ceram. Soc. 98[9] (2015) 2796-2802.
4. J. Xie, X. Mao, X. Li, B. Jiang, and L. Zhang, Ceram. Int. 43[1] (2017) 40-44.
5. B.H. Kear, R. Sadangi, V. Shukla, T. Stefanik, and R. Gentilman, Proc. of SPIE 5786 (2005) 227-233.
6. J. Wang, L. Zhang, D. Chen, E.H. Jordan, and M. Gell, J. Am. Ceram. Soc. 95[3] (2012) 1033-1037.
7. D.C. Harris, L.R. Cambrea, L.F. Johnson, R.T. Seaver, M. Baronowski, R. Gentilman, C.S. Nordahl, T. Gattuso, S. Silberstein, P. Rogan, T. Hartnett, B. Zelinski, W. Sunne, E. Fest, W.H. Poisl, C.B. Willingham, G. Turri, C. Warren, M. Bass, D.E. Zelmon, and S.M. Goodrich, J. Am. Ceram. Soc. 96[12] (2013) 3828-3835.
8. K. Morita, B.-N. Kim, K. Hiraga, and H. Yoshida, Scr. Mater. 58[12] (2008) 1114-1117.
9. K.T. Kim, T. Min, and D.W. Kim, J. Korean Powder Metall. Inst. 23[4] (2016) 263-269.
10. J.-K. Han, D.-W. Shin, B. Madavali, and S.-J. Hong, J. Korean Powder Metall. Inst. 24[2] (2017) 115-121.
11. S. Xu, J. Li, H. Kou, Y. Shi, Y. Pan, and J. Guo, Ceram. Int. 41[2] (2015) 3312-3317.
12. D.T. Jiang and A.K. Mukherjee, J. Am. Ceram. Soc. 93[3] (2010) 769-773.
13. L. Huang, W. Yao, J. Liu, A.K. Mukherjee, and J.M. Schoenung, Scr. Mater. 75 (2014) 18-21.
14. B.-N. Kim, K. Hiraga. K. Morita, and H. Yoshida, Scr. Mater. 57 (2007) 607-610.
15. R. Apetz, M.P.B. and van Bruggen, J. Am. Ceram. Soc. 86[3] (2003) 480-486.
16. B.-N. Kim, K. Higara, K. Morita, and H. Yoshida, J. Eur. Ceram. Soc. 29[2] (2009) 323-327.
17. K. Morita, B.-N. Kim, H. Yoshida, and K. Hiraga. J. Am. Ceram. Soc. 92[6] (2009) 1208-1216.
18. H.J. Ma, W.K. Jung, C. Baek, and D.K. Kim, J. Eur. Ceram. Soc. 37[15] (2017) 4902-4911.
19. J. Koike, S. Tashima, S. Wakiya, K. Maruyama, and H. Oikawa, Mater. Sci. Eng. A220[1-2] (1996) 26-34.